Propagation of Coastal-Trapped Waves at Low Latitudes in a Stratified Ocean with Continental Shelf Slope

NOBUO SUGINOHARA

Geophysical Institute, Faculty of Science, University of Tokyo, Tokyo 113, Japan

(Manuscript received 6 November 1980, in final form 4 May 1981)

ABSTRACT

Poleward propagation of coastal-trapped waves induced by a baroclinic equatorial Kelvin wave incident on the eastern boundary is studied in numerical models. When the thermocline is shallower than shelf depth and so intersects a vertical coastal wall, a coastal-trapped, internal Kelvin-type wave keeps propagating poleward. The only change in its structure is that its trapping width decreases in accordance with the decrease in the local deformation radius. On the other hand, when the thermocline intersects a continental slope, which represents a typical situation for the eastern tropical Pacific, baroclinic disturbances decrease in amplitude as they propagate poleward, and eventually disappear at middle latitudes. Transformation of the baroclinic disturbances to quasi-barotropic shelf waves takes place. Part of the barotropic energy leaks away from the coastal region in the form of barotropic Rossby waves. As the period (wavelength) of an incident equatorial Kelvin wave increases, baroclinic disturbances propagate farther poleward.

1. Introduction

The importance of the equator as a wave guide is well recognized (e.g., Moore and Philander, 1977). In the equatorial Pacific, the most dramatic phenomenon is El Niño during which anomalously warm surface water extends from the Equadorian to the Peruvian coasts. This event cannot be explained by a change in the local wind stress off Peru but may be the results of relaxation of the southeast trades over the western and central equatorial Pacific (Wyrtki, 1975). Theoretical models of Hurlburt *et al.* (1976), McCreary (1976) and Kindle (1979) support this idea. Baroclinic equatorial Kelvin waves generated in the western and central equatorial Pacific propagate eastward along the equator and finally hit the coast of South America. On the coast, the incident equatorial Kelvin waves are partially reflected back into the equatorial wave guide and partially transmitted north and south along the coast as coastal trapped internal Kelvin waves. Consequently, the coastal trapped internal Kelvin waves cause El Niño.

In addition to the theoretical model results, there is observational evidence for the propagation of baroclinic disturbances along the coast of Peru (Smith, 1978). These baroclinic disturbances are poorly correlated with local winds off Peru. The equatorial wave guide is a reliable candidate for the region of their origin. Thus, remote forcing may play an important role in dynamics of the coastal regions off North and South America through the equatorial and coastal wave guides. However, there is evidence that poleward propagation of baroclinic disturbances is limited to low latitudes (Enfield and Allen, 1980). Hence, it is desirable to know how far from the equator the baroclinic disturbances can propagate.

Wang (1975) and Allen (1975) studied the coastal trapped waves in a two-layer model in which an interface is shallower than shelf depth and intersects a vertical coastal wall. They described the possible waves in terms of barotropic shelf and internal Kelvin waves. Resonance takes place when the phase speeds of those waves are identical, and then wave characteristics are interchangeable. As an extension of these studies, Allen and Romea (1980) looked at the poleward propagation of the coastal trapped waves at low latitudes in which the variation of the Coriolis parameter is taken into account. They showed that an internal Kelvin wave propagating poleward from the equatorial region transforms to a barotropic shelf wave at a latitude where resonance takes place. Their theory thus shows how energy in coastal-trapped baroclinic disturbances may propagate efficiently from the equatorial region to middle latitudes where it eventually takes the form of barotropic shelf waves.

Wang and Mooers (1976) and Huthnance (1978) considered a continuously stratified case in which the thermocline intersects a continental slope. They found that the identification of modes as internal Kelvin or barotropic shelf waves is not always clear, i.e., in general the possible waves involve both the topographic and stratified elements of the situation. Huthnance (1978) demonstrated that wave char-

0022-3670/81/081113-10$06.50
© 1981 American Meteorological Society

Unauthenticated | Downloaded 12/08/22 01:59 PM UTC

acteristics depend on the ratio of the internal radius of deformation (L_R) to the characteristic width of the slope (L_S). Waves associated with considerable thermocline displacements exist when $L_R/L_S > 1$, but do not when $L_R/L_S < 1$. It should be remarked that resonance between barotropic shelf and internal Kelvin waves does not take place for this thermal structure.

In the present study, poleward propagation of coastal trapped waves induced by a baroclinic equatorial Kelvin wave incident on the eastern boundary is investigated numerically. Two case studies are discussed. In the first case, the thermocline is shallower than shelf depth and so intersects a vertical coastal wall. It is studied to determine whether or not the effect of resonance is effective in transferring energy. In the second case, the thermocline intersects a continental slope. For this case, we may expect that baroclinic disturbances transform to shelf waves. This is because a larger value of the Coriolis parameter yields the smaller radius of deformation relative to the characteristic width of the shelf-slope at middle latitudes.

2. Model

We consider a stratified ocean adjacent to the meridional eastern boundary in the Northern Hemisphere. The southern boundary is placed at the equator. The ocean is bounded also by artificial northern and western boundaries. The model ocean is driven by a baroclinic equatorial Kelvin wave coming through the western boundary. Schematic views of the model oceans for case A and for case B are shown in Fig. 1 and Fig. 4, respectively. We use a rectangular coordinate system on an equatorial β-plane with x eastward, y northward and z vertically downward from the mean sea surface level. Let u, v and w be the components of velocity in the x, y and z directions, respectively, P pressure and ρ density. The equations of motion and the hydrostatic relation under the Boussinesq approximation are

$$\frac{\partial u}{\partial t} + \frac{\partial u^2}{\partial x} + \frac{\partial uv}{\partial y} + \frac{\partial uw}{\partial z} - fv = -\frac{1}{\rho_0}\frac{\partial P}{\partial x} + A_V\frac{\partial^2 u}{\partial z^2} + A_H\nabla^2 u,$$

$$\frac{\partial v}{\partial t} + \frac{\partial uv}{\partial x} + \frac{\partial v^2}{\partial y} + \frac{\partial vw}{\partial z} + fu = -\frac{1}{\rho_0}\frac{\partial P}{\partial y} + A_V\frac{\partial^2 v}{\partial z^2} + A_H\nabla^2 v,$$

$$0 = -\frac{\partial P}{\partial z} + \rho g,$$

and the equation of continuity is

$$\frac{\partial u}{\partial x} + \frac{\partial v}{\partial y} + \frac{\partial w}{\partial z} = 0,$$

where A_V and A_H are the coefficients of the vertical and horizontal eddy viscosity, respectively, ρ_0 the mean density over the whole depth, and f $(=\beta y)$ the Coriolis parameter. The equation of density under the assumption that density and temperature have a linear relation is

$$\frac{\partial \rho}{\partial t} + \frac{\partial \rho u}{\partial x} + \frac{\partial \rho v}{\partial y} + \frac{\partial \rho w}{\partial z} = K_V\frac{\partial^2 \rho}{\partial z^2} + K_H\nabla^2\rho,$$

where K_V and K_H are the coefficients of the vertical and horizontal eddy diffusion, respectively.

At the initial state, the ocean is at rest and the stratification is horizontally uniform. The initial stratification, especially the depth of the thermocline, for each of the two cases will be described in the next section.

Along the western boundary, temporal variations of density and the associated, geostrophic zonal flow are prescribed, i.e.,

$$\rho = \rho_A'(z)\exp\left(-\frac{1}{2}\frac{\beta}{C_1}y^2\right)\sin(2\pi/T)t + \bar{\rho}(z),$$

$$f\frac{\partial u}{\partial z} = -g\frac{\partial \rho}{\partial y},$$

where C_1 is the phase speed for the first baroclinic mode, T the period and $\bar{\rho}(z)$ the density at the initial (basic) state. Only the first baroclinic mode (for the linear wave dynamics) is taken into account. The amplitude $\rho_A'(z)$ at the thermocline is ~ 0.7 in σ_t units and is fixed for each of the following case studies. No transport through the western boundary is allowed. The above conditions may describe the first baroclinic equatorial Kelvin wave coming into the model ocean. The conditions for the other boundaries are as follows. The east, north and south walls are free-slip boundaries, i.e., only the normal component of velocity is zero. At the equator north-south symmetry is required: $v = 0$. At the sea surface the wind stress is not considered. The bottom is a free-slip boundary. On the side walls, sea surface and bottom, the normal gradient of density is zero so that there is no heat flux across these boundaries. Setting $w = 0$ at the sea surface leads to the rigid-lid approximation. Then it is possible to define a transport streamfunction

$$\int (u, v)dz = \left(-\frac{\partial \psi}{\partial y}, \frac{\partial \psi}{\partial x}\right),$$

where the integral is performed from the mean sea surface level to the bottom. The boundary condition for the streamfunction is that the side wall is a streamline, i.e., $\psi = 0$ along the walls.

Unauthenticated | Downloaded 12/08/22 01:59 PM UTC

The numerical method used in the present experiment is basically similar to that described in Bryan (1969). One difference is that for the deepest layer, the vertical grid intervals are changed in size to fit the configuration of the slope, which is portrayed by a smoothed curve (see Figs. 1 and 4).

The following values are used for the numerical calculation: $\rho_0 = 1.0\ \mathrm{g\ cm^{-3}}$, $\beta = 3 \times 10^{-13}\ \mathrm{cm^{-1}\ s^{-1}}$, $A_V = 10\ \mathrm{cm^2\ s^{-1}}$, $A_H = 10^7\ \mathrm{cm^2\ s^{-1}}$, $K_V = 0.01\ \mathrm{cm^2\ s^{-1}}$ and $K_H = 10^3\ \mathrm{cm^2\ s^{-1}}$. In order not to smooth out the initial density stratification, the coefficients of diffusion are taken to be as small as possible. Also, to avoid penetration of short Rossby waves from the western boundary into the model ocean, the large value for A_H is used. Grid intervals are 10 km in the east–west direction and 40 km in the north–south direction. The vertical resolution is different for the two cases and will be described in the next section.

3. Results

a. Case A: The thermocline intersects a vertical coastal wall

A schematic view of the model ocean is shown in Fig. 1. The ocean has a continental shelf slope which is uniform in the alongshore direction. The width of the shelf slope is 160 km. The latitudinal width of the ocean is 600 km and the longitudinal width is 3520 km. The thermocline intersects the vertical coastal wall, and 9 levels are taken for the vertical resolution (see the bottom of Fig. 1).

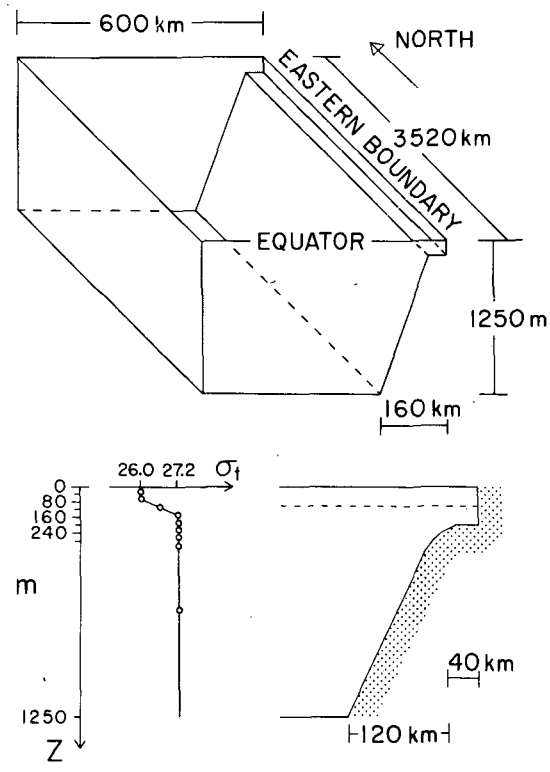

FIG. 1. Schematic view of the model ocean for case A. Initial stratification and bottom topography are plotted at the bottom.

We will describe the results for the case in which the period of the prescribed, first baroclinic, equatorial Kelvin wave passing through the western boundary is 20 days. The phase speed of the equatorial Kelvin wave (C_1) is $\sim 100\ \mathrm{cm\ s^{-1}}$, and hence the wavelength is 1700 km. Fig. 2 shows sequential patterns of the density, vertical velocity and streamfunction. The patterns of the density and vertical velocity plotted in the figure represent well the behaviors of the thermocline. The equatorial Kelvin wave propagates eastward. When this baroclinic wave passes over the continental slope, a vortex in the streamfunction field is formed and propagates poleward as a quasi-barotropic shelf wave. The propagation speed is almost identical to the phase speed (group velocity) predicted from the barotropic shelf wave theory ($\sim 105\ \mathrm{cm\ s^{-1}}$ at 800 km from the equator). For higher latitudes, the speed becomes higher, being in proportion to the value of the Coriolis parameter. A part of the energy leaks away from the coastal region as barotropic Rossby waves. The generation may be understood qualitatively from the vorticity equation for the depth-mean flow,

$$\frac{\partial \zeta}{\partial t} \sim \frac{f}{D} u_B \frac{\partial D}{\partial x}, \qquad (3.1)$$

where ζ is vorticity, D the depth and u_B the zonal flow at the bottom below the thermocline.

When the equatorial Kelvin wave hits the coast, baroclinic disturbances are induced along the coast. These disturbances are in the form of a coastal-trapped internal Kelvin wave. This wave keeps propagating poleward decreasing the trapping width in accordance with the decrease in the local radius of deformation. No remarkable decrease in amplitude of the density or vertical velocity fluctuations is observed. The internal Kelvin-type wave does not transform to a shelf wave even after it passes through the resonant latitude (~800 km from the equator).

Fig. 3 shows velocity fields at the day 30, which represent typical flow patterns for coexistence of the barotropic Rossby, shelf and internal Kelvin-type waves. On the shelf, flows associated with the internal Kelvin-type wave are clearly observed ~900 km from the equator. Even north of the resonant latitude, motions associated with the baroclinic disturbances indicate the internal Kelvin-type wave.

To check this result a two-layer model, like that of Suginohara (1974), was also studied. The period of the input equatorial Kelvin wave and the mean depth of the interface were varied in several numerical experiments. In every case of these, the internal Kelvin-type wave keeps propagating poleward. Nothing particular takes place. A significant energy

Unauthenticated | Downloaded 12/08/22 01:59 PM UTC

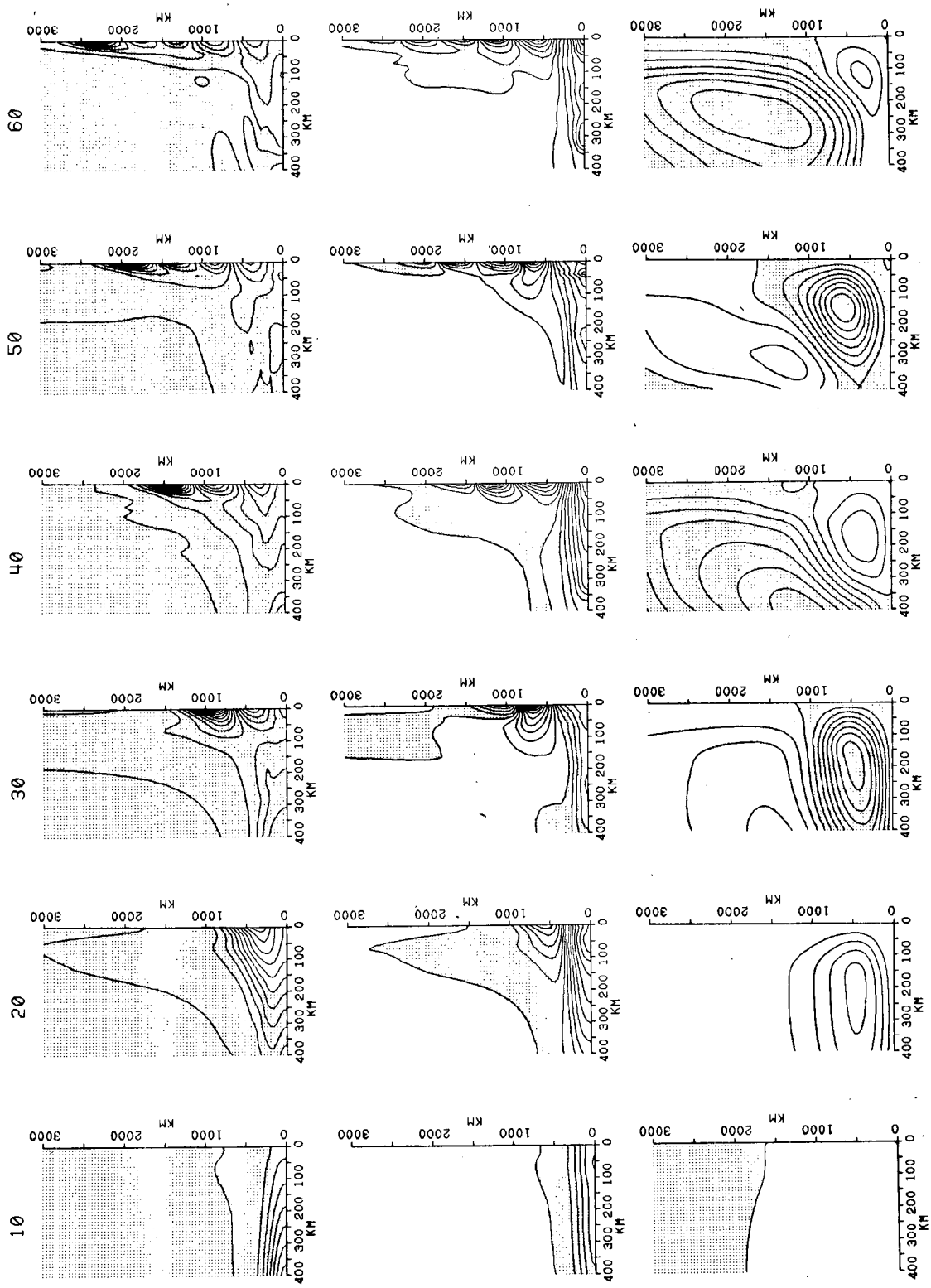

FIG. 2. Sequential patterns of the density at the depth of 100 m (top), the vertical velocity at 120 m (middle) and the streamfunction (bottom) at days 10, 20, 30, 40, 50 and 60 for case A. The contour intervals are 0.02 in σ_t units, 0.5×10^{-3} cm s^{-1} and 25×10^{10} cm^3 s^{-1} for the density, vertical velocity and streamfunction, respectively. Shaded areas indicate negative values for the vertical velocity and streamfunction, and values < 26.7 in σ_t units for the density.

Unauthenticated | Downloaded 12/08/22 01:59 PM UTC

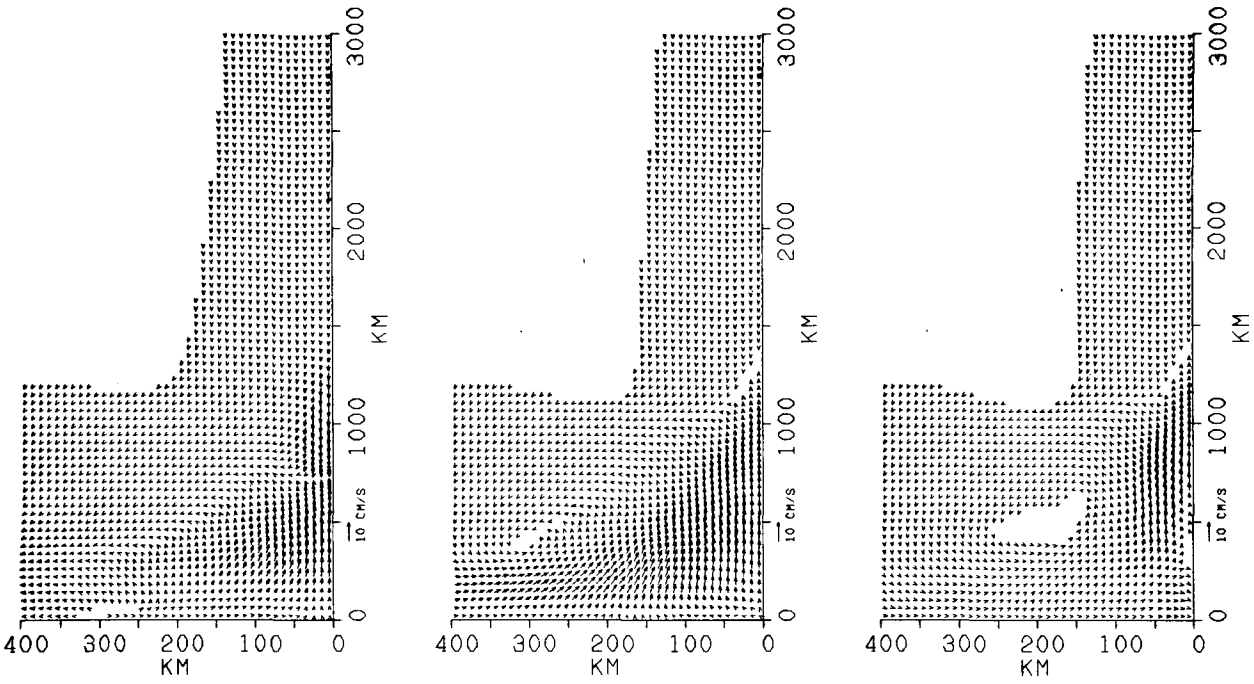

FIG. 3. Velocity fields at depths of 20 m (left), 100 m (center) and 180 m (right) at day 30 for case A.

transfer from the internal Kelvin to shelf waves induced by the effect of resonance as predicted by Allen and Romea (1980) does not take place.

b. *Case B: The thermocline intersects a continental slope*

A schematic view of the model ocean is shown in Fig. 4. The horizontal dimension of the ocean is the same as in case A. For this case there is no notable continental shelf. The thermocline intersects the continental slope, and six levels are taken for the vertical resolution (see the bottom of Fig. 4). Two cases for different periods of the prescribed, first baroclinic, equatorial Kelvin wave, i.e., 20 days and 60 days, will be discussed. The phase speed of the equatorial Kelvin wave (C_1) is $\sim$110 cm s^{-1}, and hence the wavelengths are 1900 and 5700 km.

Fig. 5 shows sequential patterns of the variables for the case of 20-day period. As in case A, the equatorial Kelvin wave induces a vortex in the streamfunction field on the slope when it passes over the slope. The vortex spreads poleward and westward as quasi-barotropic shelf and barotropic Rossby waves. Baroclinic disturbances are formed along the coast near the equator, when the equatorial Kelvin wave hits the coast; they are in the form of an internal Kelvin-type wave at the lower latitudes. In contrast to case A, the baroclinic disturbances decrease in amplitude as they propagate poleward, and disappear $\sim$1500 km from the equator.

In order to illustrate properties of the baroclinic disturbances, distributions of the streamfunction, zonal velocity and density along the meridian 30 km offshore from the coast are plotted in Fig. 6. The plotted zonal velocity well represents the flow below the thermocline. The density profiles show a con-

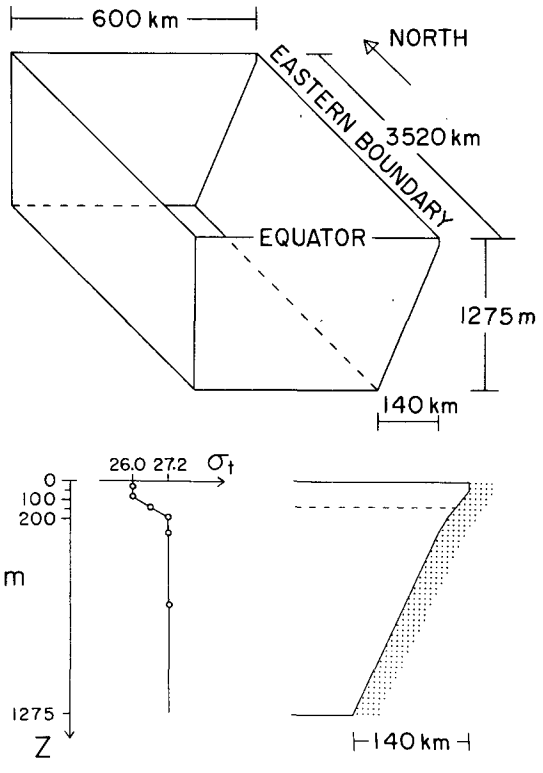

FIG. 4. Schematic view of the model ocean for case B.

Unauthenticated | Downloaded 12/08/22 01:59 PM UTC

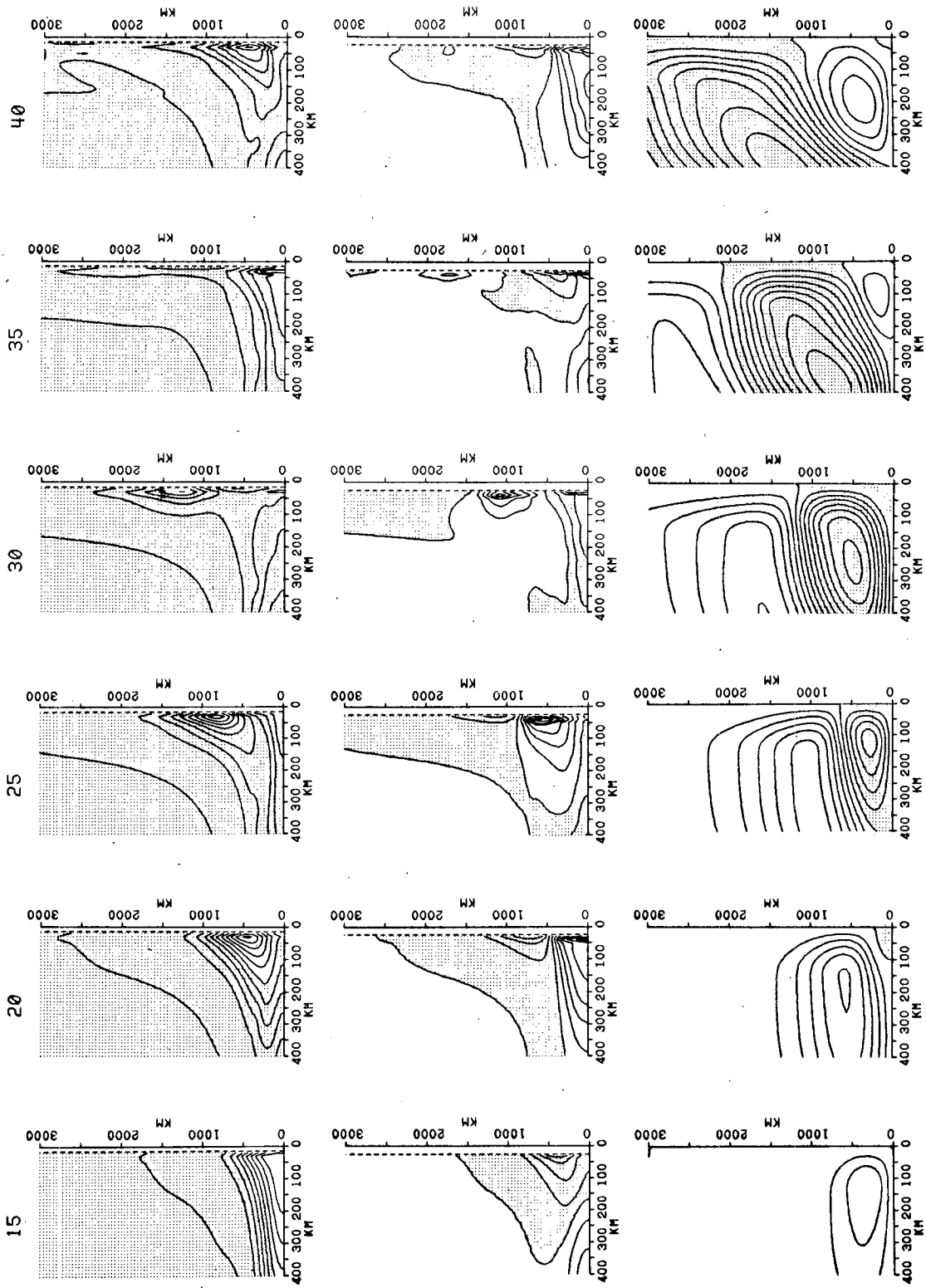

FIG. 5. Sequential patterns of the density at the depth of 125 m (top), the vertical velocity at 150 m (middle), and the streamfunction (bottom) at days 15, 20, 25, 30, 35 and 40 for case B with 20-day period. The contour intervals are 0.02 in σ_t units, 1.0×10^{-3} cm s^{-1} and 25×10^{10} cm^3 s^{-1} for the density, vertical velocity and streamfunction, respectively.

Unauthenticated | Downloaded 12/08/22 01:59 PM UTC

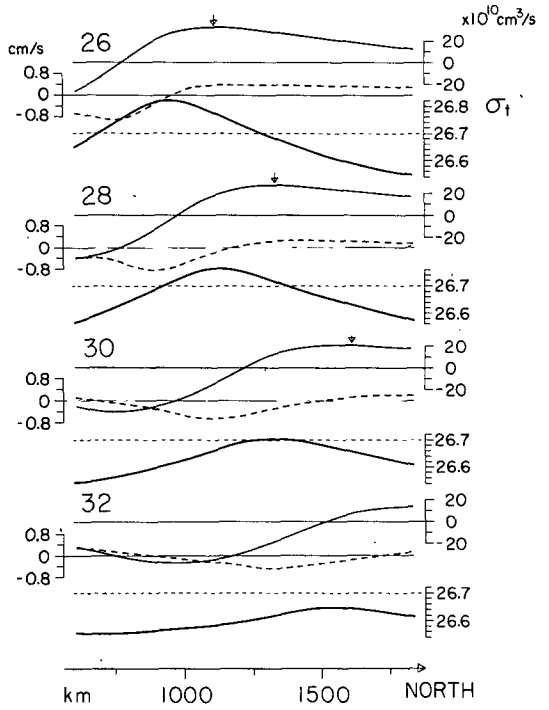

FIG. 6. Meridional distributions of the streamfunction (thin line), zonal velocity at 125 m (dashed line) and density at 125 m (bold line) along a section 30 km offshore from the coast at days 26, 28, 30, 32, for case B with 20-day period. Arrows indicate positions of peaks in the streamfunction profiles.

spicuous decrease in amplitude from day 26 through day 32. The propagation speed during these days is roughly 100 cm s^{-1}. The peaks in the streamfunction profiles lie close to those in the density profiles from day 26 through 30, and their propagation speed is almost identical to that for the density. This value is smaller than the phase speed (group velocity) predicted from barotropic shelf wave theory (~140 cm s^{-1} at 1200 km from the equator). This apparent retardation may be caused by the local generation of the transport, i.e., energy is being transferred from the internal Kelvin-type wave to the quasi-barotropic shelf wave. After the baroclinic disturbances considerably decrease in amplitude, the propagation speed for the streamfunction increases as seen at days after day 30 (see also Fig. 5). Examination of the distribution of the zonal flow below the thermocline also indicates this energy transfer. During a period when remarkable baroclinic disturbances are left (days 26–30), the direction of the zonal flow depends mainly on the density distribution, i.e., it is in geostrophic balance with the density field. The flow which feels the slope generates a vortex as understood from the relation, (3.1). Although this relation indicates only a tendency for vortex generation, an anticyclonic vortex does generate in the region where u_B has a positive sign. Therefore, it may be concluded that energy transfer from the baroclinic disturbances to shelf waves takes place, and the baroclinic disturbances eventually disappear.

Fig. 7 shows velocity fields at day 25, which represent typical flow patterns for this case. In spite of the remarkable baroclinic disturbances found ~800 km from the equator, motions associated with quasi-barotropic shelf waves dominate in the northern half of the disturbances.

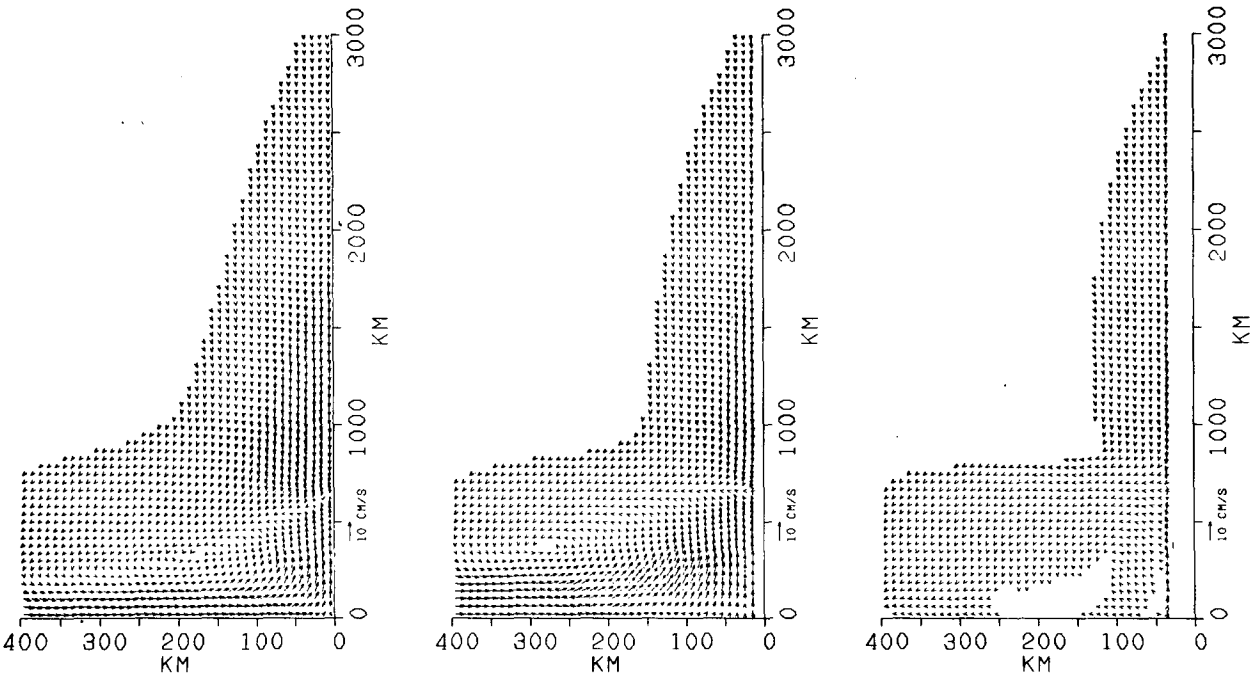

FIG. 7. Velocity fields at depths of 25 m (left), 125 m (center) and 225 m (right) at day 25 for case B with 20-day period.

Unauthenticated | Downloaded 12/08/22 01:59 PM UTC

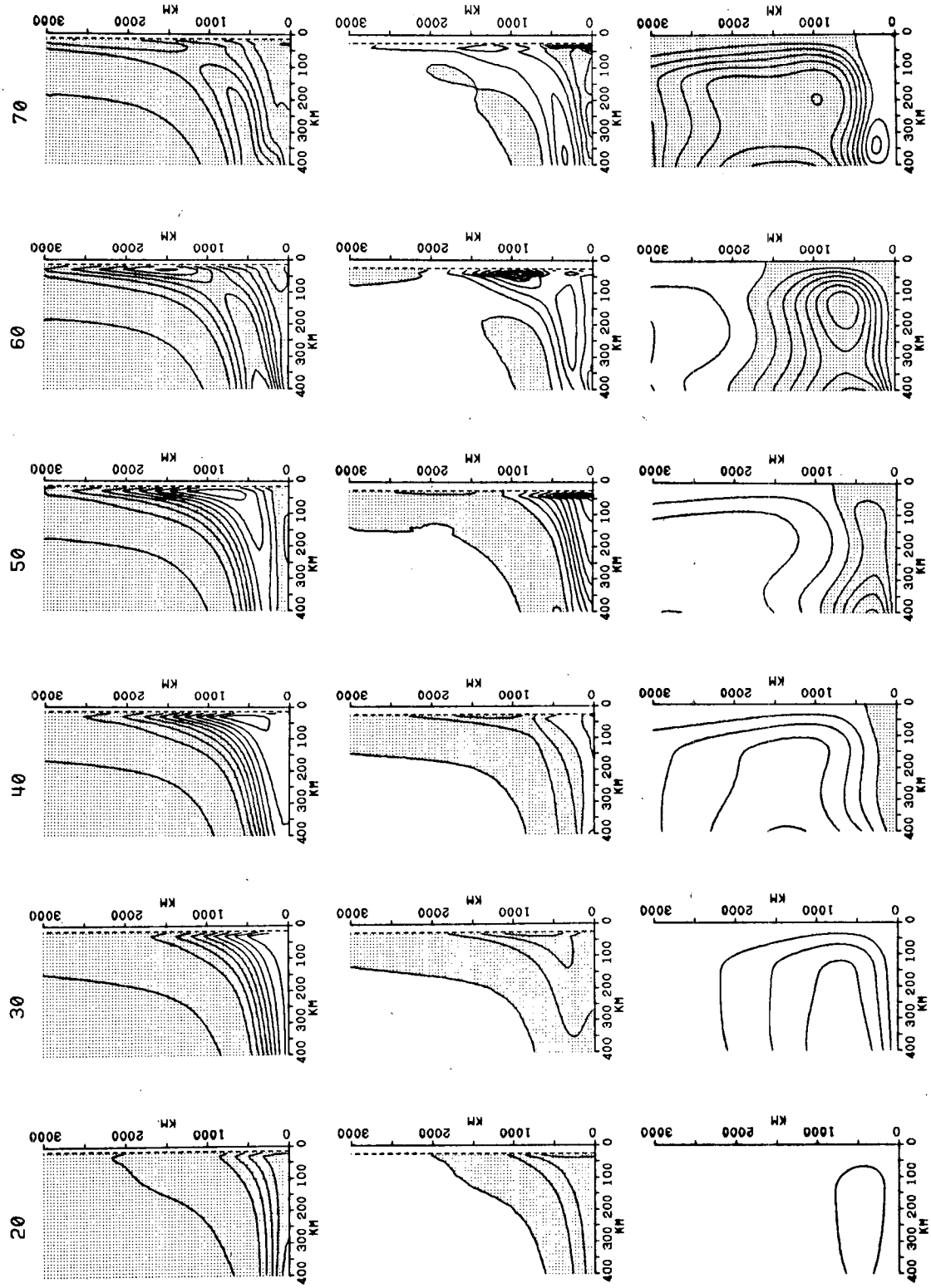

FIG. 8. As in Fig. 6 except for case B with 60-day period at days 20, 30, 40, 50, 60 and 70 (the contour interval for vertical velocity is 0.4×10^{-3} cm s^{-1}).

Unauthenticated | Downloaded 12/08/22 01:59 PM UTC

The results for the case of 60-day period are shown in Fig. 8. The baroclinic disturbances decrease in amplitude as they propagate poleward, and disappear at ~2000 km from the equator. The apparent retardation of propagation for the flow patterns of the streamfunction caused by the local generation of the shelf wave is evident (cf. Fig. 2). The baroclinic disturbances propagate farther poleward than those for the case of 20-day period. An additional case study for 40-day period leads to a conclusion that the baroclinic disturbances can propagate farther poleward, as the period (wavelength) of the input equatorial Kelvin wave increases. Effects of β are more clearly observed for the longer period cases. The westward propagation of the internal equatorial Rossby waves is found in the density fields from day 50 to day 70 in Fig. 8. For the flow patterns of the streamfunction, leakage of the barotropic motions from the coastal area by barotropic Rossby waves is clearly observed.

In each of the cases, balances for the momentum and vorticity equations are almost linear. For the equation of density, a balance, $\partial\rho/\partial t + w[\partial\bar{\rho}(z)/\partial z] \approx 0$ dominates. Thus, the results can be described by the linear wave dynamics.

4. Discussion and conclusion

Poleward propagation of the coastal trapped waves induced by a baroclinic equatorial Kelvin wave incident on the eastern boundary has been studied in numerical models. For the case in which the thermocline is shallower than shelf depth and so intersects the vertical coastal wall, the internal Kelvin-type wave keeps propagating poleward. The only change in its structure is that its trapping width decreases in accordance with the decrease in the local radius of deformation. The effect of resonance is insignificant. The internal Kelvin-type wave does not transform to the barotropic shelf wave at the latitude where the resonance takes place, which disagrees with the result of Allen and Romea (1980). The insignificant effect of the resonance may be intuitively understood by a mechanical analog: a coupled harmonic oscillator problem. Let us consider a case where one oscillator is initially set in motion. Resonance yields the most efficient way to transfer energy from one oscillator to the other through coupling. However, it takes time for energy to reach the other oscillator; this time is proportional to the beat period $2/|\omega_1 - \omega_2|$, where ω_1 and ω_2 are natural frequencies of the two oscillators. Next, let us apply this fact to the wave problem of a two-layer ocean. If we follow a particular crest of the internal Kelvin wave, the crest takes a short time to pass through the band in which the condition for resonance and near-resonance is satisfied. The difference in frequencies between the internal Kelvin and shelf waves is quite small compared with either of these waves (Allen, 1975). The beat period is much longer than the time needed for the internal Kelvin wave to pass through the band. Thus, we cannot expect that a substantial amount of energy is transferred from the internal Kelvin to shelf waves by resonance. Therefore, the internal Kelvin waves keep propagating poleward, passing through the resonant latitude, and only losing a very small amount of energy.

On the other hand, for the case in which the thermocline intersects the continental slope, the baroclinic disturbances decrease in amplitude as they propagate poleward, and eventually disappear. As the period (wavelength) of the incident equatorial Kelvin wave increases, the baroclinic disturbances generated near the equator can propagate farther poleward. The propagation speed of the shelf wave and the zonal flow below the thermocline indicate that the energy of the baroclinic disturbances is transferred to the shelf wave. This may correspond to the adjustment process of the coastal trapped waves to a new environment created by the change in the Coriolis parameter. Waves associated with considerable thermocline displacements, internal Kelvin-type wave, exist at low latitudes, but do not at middle latitudes (Huthnance, 1978). Thus, the baroclinic disturbances eventually must transform to quasi-barotropic shelf waves. Part of the energy leaks away from the coastal region in the form of barotropic Rossby waves.

The observed thermocline intersects the continental slope in the eastern tropical Pacific (see, e.g., Smith, 1978). It may be expected to occur in a real ocean that baroclinic disturbances from the equatorial region does not propagate poleward beyond the latitudes which depend on the period (wavelength) of them. The results of the data analysis by Enfield and Allen (1980) may be explained by the present mechanism. However, to substantiate the present study for application to the real ocean, the bottom topography and the basic stratification similar to those observed need to be taken into account. At the same time, detailed study of coastal-trapped wave modes under observed circumstances is required.

Another purpose of the present study has been to discuss effects of a continental shelf slope on transmission of energy from an incident equatorial Kelvin wave to coastal trapped baroclinic disturbances. Additional experiments (not shown here) show that baroclinic disturbances induced by an incident equatorial Kelvin wave for the case with a shelf slope are only a few percent smaller than those for the case with no shelf slope. Thus, there is no significant effect of the shelf slope on this transmission. However, the importance of the shelf slope should be emphasized for understanding the whole dynamics in the tropical ocean, because coastal-trapped baro-

Unauthenticated | Downloaded 12/08/22 01:59 PM UTC

clinic disturbances (coastal-trapped Kelvin-type waves) induced by the incident equatorial Kelvin wave transforms to quasi-barotropic shelf waves, as was found for case B. Moore (1968) and Cane and Sarachik (1977) showed that for a flat bottom ocean the coastal trapped Kelvin-type wave plays an essential role on reflection at the coast. The transformation of the baroclinic Kelvin-type wave to quasi-barotropic shelf waves alters the characteristics of reflections. Moreover, part of energy in the baroclinic equatorial Kelvin wave is eventually reflected back to the deep ocean as barotropic Rossby waves. The reflection problem including the effects of the continental shelf slope needs to be studied.

Acknowledgments. I would like to thank Drs. K. Kajiura, M. Kubota and M. Fukasawa for pleasant discussions. Thanks are extended to Drs. M. Tsuchiya and J. H. Yoon for reading the manuscript and making very helpful comments. I thank also Ms. T. Osada for drafting the figures and typing the manuscript.

REFERENCES

Allen, J. S., 1975: Coastal trapped waves in a stratified ocean. *J. Phys. Oceanogr.*, **5**, 300–325.

——, and R. D. Romea, 1980: On coastal trapped waves at low latitudes in a stratified ocean. *J. Fluid Mech.*, **98**, 555–585.

Bryan, K., 1969: A numerical method for the study of ocean circulation. *J. Comput. Phys.*, **4**, 347–376.

Cane, M. A., and E. S. Sarachik, 1977: Forced baroclinic ocean motions, II. The linear equatorial bounded case. *J. Mar. Res.*, **35**, 395–432.

Enfield, D. B., and J. S. Allen, 1980: On the structure and dynamics of monthly mean sea level anomalies along the Pacific coast of North and South America. *J. Phys. Oceanogr.*, **10**, 557–578.

Hurlburt, H. E., J. C. Kindle and J. J. O'Brien, 1976: A numerical simulation of the onset of El Niño. *J. Phys. Oceanogr.*, **6**, 621–631.

Huthnance, J. M., 1978: On coastal trapped waves: Analysis and numerical calculation by inverse iteration. *J. Phys. Oceanogr.*, **8**, 74–92.

Kindle, J. C., 1979: Equatorial Pacific variability—Seasonal and El Niño time scale. Ph.D. thesis, Florida State University, 134 pp.

McCreary, J. P., 1976: Eastern tropical ocean response to changing wind systems: With application to El Niño. *J. Phys. Oceanogr.*, **6**, 632–645.

Moore, D. W., 1968: Planetary-gravity waves in an equatorial ocean. Ph.D. thesis, Harvard University.

——, and S. G. H. Philander, 1977: Modelling of the tropical ocean circulation. *The Sea*, Wiley-Interscience, Chap. 8.

Smith, R. L., 1978: Poleward propagating perturbations in currents and sea level along the Peru coast. *J. Geophys. Res.*, **83**, 6083–6092.

Suginohara, N.,1974: Onset of coastal upwelling in a two-layer ocean by wind stress with longshore variation. *J. Oceanogr. Soc. Japan*, **30**, 23–33.

Wang, D. P., 1975: Coastal trapped waves in a baroclinic ocean. *J. Phys. Oceanogr.*, **5**, 326–333.

——, and C. N. K. Mooers, 1976: Coastal trapped waves in a continuously stratified ocean. *J. Phys. Oceanogr.*, **6**, 853–863.

Wyrtki, K., 1975: El Niño—The dynamic response of the equatorial Pacific ocean to atmospheric forcing. *J. Phys. Oceanogr.*, **5**, 572–584.

Unauthenticated | Downloaded 12/08/22 01:59 PM UTC